Proceedings of the 2nd LAAS Conference on Computer Simulation, Beirut, Lebanon, September 1997

NUMERICAL SIMULATION OF CAVITATION DYNAMICS

Georges L. Chahine
DYNAFLOW, INC.
7210 Pindell School Road
Fulton, Maryland 20759, USA
e-mail:glchahine@dynaflow-inc.com

Abstract

Cavitation is known for its deleterious effects, namely erosion, noise and loss of performance. These effects are directly connected to the dynamics of microscopic bubble nuclei that are present in the liquid. Here, we consider the modelling and simulation of the dynamics of these nuclei at microscopic level, and extend this to large scale cavities such as on propeller blades and planing surfaces. The various aspects of the problem are highlighted and briefly addressed. New areas of research for non spherical bubbles and bubble clouds are also considered. The importance of the inclusion of collective effects and the presence non uniform flow in a realistic cavitating flow field is highlighted.

Key Words: Cavitation, Cavity Dynamics, Simulation, Boundary Element Method.

INTRODUCTION

Cavitation and bubble dynamics have been the subject of extensive research since the early works of Besant [1] and Lord Rayleigh [2]. The phenomenon has been mostly studied for hydrodynamic applications where its presence is associated with deleterious effects: namely performance deterioration, material erosion, and noise generation. More recently, cavitation has been studied for useful purposes including sound generation, cutting, drilling, cleaning, enhancement of mixing and chemical reactions, emulsification, etc. [3, 4, 5]. Cavitation is also of interest for its damaging effects on implants such as mechanical heart valves, or for its negative effects on biological cells and tissue. In all cases stresses generated by cavitation lead to energetic and destructive effects, that are difficult to predict and simulate.

This contribution will consider main aspects of the subject relevant to cavitation erosion from a microscopic point of view and then address larger macroscopic scale which are of more direct application to the engineering community. Our aim is to give an overview of the problem areas where significant knowledge has been accumulated and to also discuss aspects of the dynamics which are the subject of on-going intensive research.

CAVITATION INCEPTION

Despite a large number of publications on the subject (see for instance the reference books [6, 7]) the fundamentals of cavitation remain relatively poorly understood. In order to achieve a cavitation free design of a submerged body (such as a valve, propeller, etc.), or to simulate cavitation and test a model scale in a laboratory environment, it is necessary to establish criteria for cavitation inception, and to define scaling parameters to conserve between model and full scale. Engineers and practitioners use a definition of cavitation based on an over-simplification.. This traditional engineering definition is expressed as follows: *A liquid flow experiences cavitation if the local pressure drops below the liquid vapor pressure, p_v.*

This definition is then used to define the non-dimensional parameter characterizing cavitation inception.

Cavitation Number

A dimensional analysis of the flow around an obstacle of streamwise and transverse characteristic length scales, L and W, shows that the pressure, p_M, at any point M, can be written as a function, $\mathcal{F}$, of the following variables:

$$p_M = \mathcal{F}(P_\infty, \alpha, L, W, \rho, V_\infty, \mu), \qquad (1)$$

where α is the incidence angle of the flow relative to the obstacle, P_∞ and V_∞ are the characteristic pressure and velocity of the flow, and ρ and μ are the liquid density and kinematic viscosity. Based on the above engineering definition of cavitation, from a cavitation inception standpoint any pressure, p_M, in the liquid flow is important only in terms of the pressure difference, $p_M - p_v$, since the liquid cavitates when $p_M = p_v$. In this case, Equation (1) becomes at cavitation inception:

$$\frac{P_\infty - p_v}{\frac{1}{2}\rho V_\infty^2} = \mathcal{F}(\alpha, \frac{W}{L}, \frac{\rho V_\infty L}{\mu}), \text{or } \sigma = \mathcal{F}(\alpha, \mathcal{G}, \mathcal{R}_e). \qquad (2)$$

$\mathcal{R}_e$ is the Reynolds number, $\mathcal{G}$ is a geometric characteristic (shape parameter) of the obstacle, and σ is the "*cavitation number*" defined as:

$$\sigma = \frac{P_\infty - p_v}{\frac{1}{2}\rho V_\infty^2}. \qquad (3)$$

Scaling various cavitation experiments or a model to a full scale is obtained by conserving σ. In fact, the above definition of cavitation inception is only true in static conditions when the liquid is in contact with its vapor through the presence of a large free surface. For the more common condition of a liquid in a flow, liquid vaporization can only occur through the presence of "micro free surfaces" or microbubbles, also called "cavitation nuclei". Indeed, a pure liquid free of nuclei can sustain very large tensions, in the hundreds of atmospheres, before a cavity can be generated through separation of the liquid molecules [6]. Therefore, it is these nuclei that will respond to the liquid pressure dynamically by oscillating and eventually *growing explosively* (i.e. *cavitate*).

Bubble Static Equilibrium

The first level of sophistication for the definition of a cavitation inception criterion is based on the static equilibrium of a spherical bubble

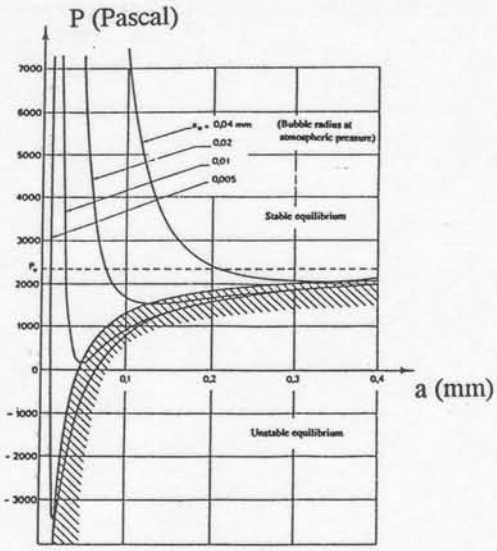

Figure 1: Curves of Bubble Static Equilibrium

in a liquid. The bubble is assumed to contain non condensable gas of partial pressure, P_g, and vapor of the liquid of partial pressure, p_v. Therefore, the balance between the internal pressure, the liquid pressure, P_{Lo}, and surface tension, γ, can be written:

$$P_{Lo} = p_v + P_{g_o} - \frac{2\gamma}{R_o}, \qquad (4)$$

where R_o is the bubble radius.

If the liquid ambient pressure changes slowly, the bubble radius will adapt. The vaporization of the liquid at the bubble / liquid interface occurs very fast relative to the time scale of the bubble dynamics, so that the liquid and its vapor can be considered at equilibrium at every instant, with P_{g_o} remaining constant. On the other hand, gas diffusion occurs much slower, so that the amount of gas inside the bubble remains constant. This results in a gas partial pressure which varies with the bubble volume as follows:

$$P_g = P_{g_o}\left(\frac{R_o}{R}\right)^3, \qquad (5)$$

where P_{g_o} is the reference gas pressure.

The dynamic equation at the bubble wall then becomes:

$$P_L(R) = P_v + P_{g_o}\left(\frac{R_o}{R}\right)^3 - \frac{2\gamma}{R}. \qquad (6)$$

An understanding of the bubble stable equilibrium can be obtained by considering the curve, $P_L(R)$. As illustrated in Figure 1, this curve has a minimum below which there is no equilibrium bubble radius. Only the left side branch of the curve correspond to a stable equilibrium. Therefore, *if the pressure in the flow field drops below*

the minimum of the curve, or critical pressure, p_c, *an explosive bubble growth (*cavitation*) is provoked.*

This provides an improved definition for cavitation inception which depends on the size of the nuclei. The "*critical pressure*" is the minimum of $P_L(R)$:

$$p_c = p_v - \frac{4\gamma}{3r_c}, \tag{7}$$

where r_c is the '*critical radius*' given by

$$r_c = \left[\frac{3R_o^3}{2\gamma}\left(P_{Lo} - p_v + \frac{2\gamma}{R_o}\right)\right]^{1/2}. \tag{8}$$

For a given ambient pressure, P_{Lo}, any bubble larger than r_c will cavitate. This new definition of cavitation inception highlights the fact that a correct scaling of the cavitation phenomenon has to account not only for the conservation of the cavitation number, but also for the conservation of the nuclei size distribution between the model and the full scale.

SPHERICAL BUBBLE DYNAMICS

The most commonly used bubble dynamics model is for a spherical bubble in an incompressible liquid. In this case, the radial velocity of the liquid, u_r, at a distance, r, from the bubble center, is directly related to the bubble wall velocity through the continuity equation:

$$u_r = \overset{\circ}{R}(t)\left[\frac{R(t)}{r}\right]^2, \tag{9}$$

where $\overset{\circ}{R}(t)$ is the bubble wall velocity at time t. This equation accounts for the kinematic condition at the bubble wall. A second boundary condition at the bubble wall, expresses the balance of the normal stresses,

$$P_L(R) + 4\mu\frac{\overset{\circ}{R}}{R} = P_i - \frac{2\gamma}{R}, \tag{10}$$

where P_i is the pressure inside the bubble, and μ the liquid kinematic viscosity. The noncondensible gas at the partial pressure, P_g, is related to the reference value P_{g_o}, through:

$$P_g = P_{g_o}\left(\frac{\mathcal{V}_o}{\mathcal{V}}\right)^k, \tag{11}$$

where the constant k is between 1.0 (isothermal) and c_p/c_v (adiabatic), and $\mathcal{V}_o$ and $\mathcal{V}$ are the reference and instantaneous bubble volume.

A number of effects such as gas diffusion or heat transfer have been neglected in Equation (10), and are usually unimportant for the case of a growing and collapsing bubble in a cold liquid. For an oscillating bubble, however, rectified diffusion can be very important.

If we replace Equation (9) in the liquid momentum equation, integrate that equation between the radius of the bubble and infinity where the imposed pressure is $P_\infty(t)$, and account for Equation (10), we obtain the well known Rayleigh-Plesset equation [2] where dots denote time derivatives:

$$\rho[R\overset{\circ\circ}{R} + \frac{3}{2}\overset{\circ}{R}^2] + 4\mu\frac{\overset{\circ}{R}}{R} = P_{g_o}\left[\frac{R_o}{R}\right]^{3k} + P_v - P_\infty(t) - \frac{2\gamma}{R}. \tag{12}$$

This equation describes the bubble radius versus time when the time variations of P_∞ are known. Time integration of this equation enables one to obtain conditions for bubble oscillations, or rapid bubble growth and collapse. In addition, this equation provides necessary input to compute the pressure generated during bubble collapse.

NONSPHERICAL BUBBLE DYNAMICS

In most practical applications, bubbles are seldom isolated or spherical. With the advent of modern computational techniques, bubble deformations bubble/bubble and bubble/flow interactions can be addressed. The method that we have developed to solve these problems is described below.

Boundary Element Method

For cavity dynamics, large but subsonic cavity wall velocities are involved and, as a result, viscous and compressible effects in the liquid can be neglected. The flow due to cavity dynamics can therefore be considered potential (velocity potential, ϕ_b), and satisfies the Laplace equation,

$$\nabla^2\phi_b = 0. \tag{13}$$

Boundary conditions are such that at rigid surfaces fluid velocities normal to the boundary equal the normal velocity of the boundary itself.

The Boundary Element Methods that we developed (2DynaFS and 3DynaFS), [8, 9, 10], use Green's equation to determine a solution of the Laplace equation. If the velocity potential, ϕ_b , and its normal derivatives are known on the fluid boundaries (points M), and ϕ_b satisfies the Laplace equation, then ϕ_b can be determined at any point P in the fluid domain using:

$$\int\int_S \left[-\frac{\partial\phi_b}{\partial n}\frac{1}{|\mathbf{MP}|} + \phi_b\frac{\partial}{\partial n}\left(\frac{1}{|\mathbf{MP}|}\right)\right] dS = a\pi\phi_b(P), \tag{14}$$

where Ω is the solid angle under which P sees the fluid. The advantage of this integral representation is that it effectively reduces by one the dimension of the problem. If P is selected to be on the boundary of the fluid domain, then a closed system of equations is obtained and used at each time step to solve for values of $\partial\phi_b/\partial n$ (or ϕ_b), assuming that all values of ϕ_b (or $\partial\phi_b/\partial n$) are known at the preceding time step.

To solve Equation (14) numerically, the initially spherical bubble is discretized into a geodesic shape with flat triangular panels. To evaluate the integrals in Equation (14) over any particular panel, a linear variation of the potential and its normal derivative over the panel is assumed.

With the problem initialized and the velocity potential known over the surface of the bubble, an updated value of $\partial\phi_b/\partial n$ can be obtained by performing the integrations expressed above and solving the corresponding matrix equation. The unsteady Bernoulli equation can then be used to solve for $D\phi_b/Dt$, the total material derivative of ϕ_b while following a particular node during its motion. Using an appropriate time step, all values of ϕ_b on the bubble surface and at all node positions can be updated. This time stepping procedure is repeated throughout the bubble oscillation period, resulting in a shape history of the bubbles.

Presence of a Basic Flow

To study bubble dynamics in a nonuniform flow field, the following model is used [10]. Denoting $\mathbf{V}_o$ the velocity of the nonuniform flow, and $\mathbf{V}_1$ the velocity field in the presence of oscillating bubbles, we define "bubble flow" velocity and pressure variables, $\mathbf{V}_b$ and P_b, as:

$$\mathbf{V}_b = \mathbf{V}_1 - \mathbf{V}_o, \qquad P_b = P_1 - P_0. \tag{15}$$

By noticing that for cavitating flows this "bubble flow" field can be considered potential, we can use a method similar to the one described in the previous section to study the dynamics. We then obtain the following modified Bernoulli equation:

$$\nabla\left[\frac{\partial\phi_b}{dt} + \frac{1}{2}|\mathbf{V}_b|^2 + \mathbf{V}_o\cdot\mathbf{V}_b + \frac{P_b}{\rho}\right] = \mathbf{V}_b\times(\nabla\times\mathbf{V}_o). \tag{16}$$

For cavitation in a line vortex this equation becomes [18,19,23]:

$$\frac{\partial\phi_b}{dt}+\frac{1}{2}|\mathbf{V}_b|^2+\frac{P_b}{\rho} = \text{constant along a radial direction.} \tag{17}$$

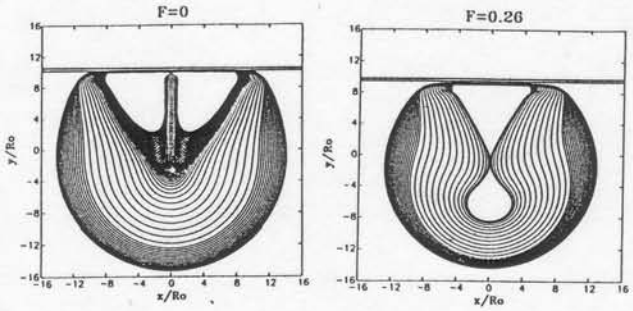

Figure 2: Numerical simulation of bubble collapse near a solid wall using 2DynaFS. Bubble contours at various times during collapse. a) No external body forces and formation of a reentering jet. b)Presence of a strong external body force and bubble splitting.

In the case of a boundary layer flow such that all velocity vectors are parallel to the wall (unit direction, $\mathbf{e}_x$), and depend only on the distance, z, to the wall, $\mathbf{V_o} = f(z).\mathbf{e}_x$, (16) becomes:

$$\frac{\partial\phi_b}{dt}+\frac{1}{2}|\mathbf{V}_b|^2+\mathbf{V}_o\cdot\mathbf{V}_b+\frac{P_b}{\rho} = \text{constant along the } y \text{ direction.} \tag{18}$$

These two expressions are used in conjunction with the numerical model described earlier to conduct the simulations shown below. This model is presently being improved using a coupling between a vortex element method and the BEM described here [14]

ILLUSTRATIVE NUMERICAL RESULTS

Behavior near a solid wall

The physical mechanisms by which bubble collapse near a solid wall causes material erosion has been the subject of research for a long time. A shock wave is generated at bubble collapse [6, 7]. In addition, bubble collapse near a solid surface can proceed with the formation of a very fast and damaging microjet. In absence of other acceleration or body forces, the bubble first elongates perpendicular to the wall during its growth phase, then the bubble side away from the wall flattens and a reentering region is formed initiating a microjet which pierces the bubble and hits the wall. Figure 2.a shows a numerical simulation of this collapse using our code 2DynaFS which illustrates the formation of the re-entering jet. Figure 3 presents some of our high speed photographs using the spark generated bubbles [13]. Other very beautiful picture of the phenomenon have been obtained by Lauterborn [12] using a laser beam to generate the bubbles.

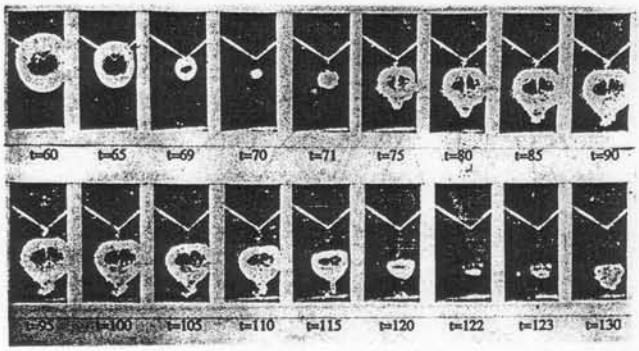

Figure 3: High speed photo of bubble collapse near a wall using a spark-generated bubble.

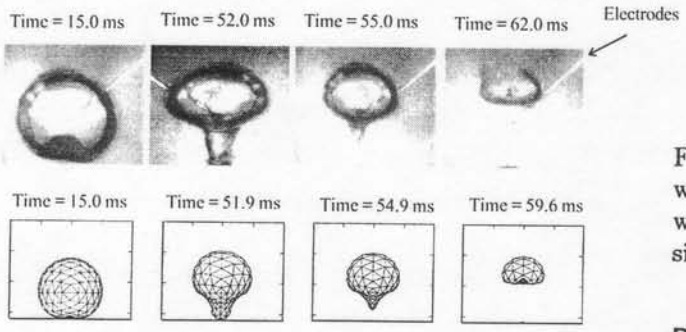

Figure 4: Bubble behavior near a wall in presence of a pressure gradient. Case where the attraction to the wall is weaker than the pressure gradient. a) high speed photo of a spark-generated bubble, and b) Simulation using 3DYNAFS

.

In presence of a body force, such as gravity or a uniform acceleration perpendicular to the wall, resulting in a pressure that decays when moving away from the wall, the attraction due to the wall is counterbalanced. Depending on the relative importance of the two forces: attraction to the solid wall and the imposed body force, the bubble shape modification can be significantly altered. When the two forces, are of the same order the bubble ends up by splitting into two parts. As shown in Figure 2.b, it thins at its central part, cuts itself into two parts which subsequently move in opposite direction. When the body force is predominant, the bubble ends up into a 'bulb' shape, and ultimately moves away from the wall. This is illustrated in Figure 4, which shows a 3DYNAFS simulation, as well as a the corresponding spark generated bubble experimental observation. The correspondence is remarkable.

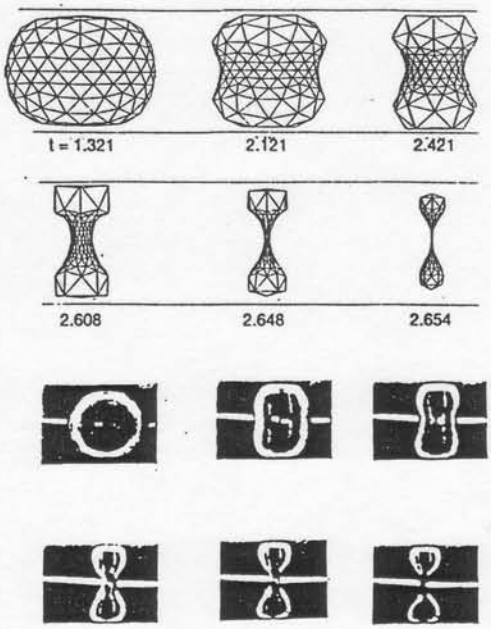

Figure 5: Bubble collpase between two soild walls. a) High speed photography observations with a spark-generated bubble. b) Numerical simulation using 3DYNAFS.

Behavior between two solid walls

The collapse of bubbles between two solid walls is interesting from a practical view point of cavitation in confined areas. The large deformations involved are also of interest from the fundamental dynamics point of view. A bubble centered at equal distance from the walls, first elongates parallel to the walls (direction of most freedom) during its growth, then perpendicularly when the implosion starts. Later the bubble constricts in the medium plane of symmetry and splits into two parts. This is observed experimentally in Figure 5.a and simulated numerically using our code 3DYNAFS in Figure 5.b. Later on each of the two bubbles formed collapses with the formation of a microjet directed to the closer wall. Quantitatively the presence of the two walls augments the bubble lifetime significantly. This lengthening effect increases dramatically when the spacing between the two walls is reduced [15].

Bubble collapse near a flat wall in a shear flow

While fundamental work on bubble dynamics has been made in a quiescent liquid near an infinite wall, it is obvious that cavitating bubbles most often occur in a flow with a slip velocity between the bubble and the liquid. These effects can be simulated numerically using 3DY-

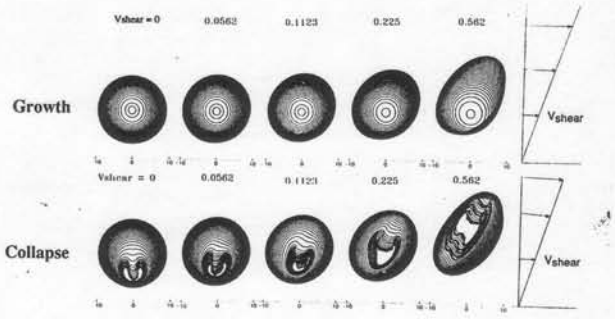

Figure 6: Influence of the presence of a linear shear velocity on the collapse of a bubble near a solid wall. V_{shear} is normalized with the Rayleigh velocity $\sqrt{\Delta P/\rho}$.

NAFS. Figure 6 illustrates the results of bubble behavior near a flat plate in the presence of a shear flow. The shear flow is such that $V_o = 0$ at the wall and grows linearly away from it to attain V_{shear} at the location of the bubble center. The figure shows interesting results for bubble behavior during bubble growth and collapse. For an increasing ratio, $\tau = V_{shear}/\sqrt{\Delta P/\rho}$, between the shear flow velocity and the characteristic bubble collapse velocity (ΔP is the pressure difference across the bubble wall), the bubble deforms and elongates more and more during its growth. For small values of τ, the re-entering jet is deviated from the perpendicular to the plate with increasing values of τ. For larger values of τ, the re-entering jet formation is totally modified and the bubble tends to cut itself into two. With increasing values of τ, an interesting lifting effect is observed, and the bubble centroid moves away from the wall. This results from an interaction between the shear flow and the rotation imparted by the velocity gradient to the bubble.

Interaction between multiple bubbles

In a practical cavitating flow field multibubble interactions need to be taken into account. The first model we developed was based on matched asymptotic expansions [16]. This model was able to explain the fact that collective bubble dynamics can generate pressures much higher than expected from simple addition of single bubble effects, resulting in much higher erosion rates observed when cloud cavitation occurs. However, this model diverged when the number of bubbles increased or when the bubble spacing decreased. Using the BEM method described here, these limitations can be removed, and more realistic and accurate results obtained. Figure 7 compares the results obtained with 3DYNAFS with those using the asymptotic approach. The bubble cloud is subjected to a sudden pressure drop, and cloud configurations of 1, 2, 4 and 8-bubbles are considered. For the 2-bubble case the bubble centers are separated by a distance l_0, and the initial gas pressure in each bubble is such that the bubble would achieve a maximum radius $R_{max} = r_{b0} = 0.047 l_0$ if isolated. The four-bubble configuration considers similar bubbles centered on the corners of a square with sides of dimension l_0. Finally, the eight bubbles are located on the corners of a cube of side l_0. The figure presents the variations with time of the pressure measured at the "cloud center" normalized by that obtained with an isolated bubble. As expected, the asymptotic approach gives a very good approximation for a small number of bubbles, N. However, the pressures predicted by the asymptotic analysis are seen to become much higher than the more accurate 3D results for an increasing value of N. Similar results are observed when the cloud void fraction or the ratio, $\epsilon = r_{bo}/l_o$, increases [9].

Figure 8 illustrates the effect of asymmetries in a bubble cloud configuration, and considers an asymmetric five bubble configuration. All bubbles have the same initial radius and internal pressure, and are initially spherical and located in the same plane. The most visible effect is that observed on the center bubble. Its growth is initially similar to that of the other bubbles, but it ends up being the least deformed. Later on, as the collapse proceeds with the development of a reentrant jet directed towards the central bubble, this bubble appears to be shielded by the rest of the cloud. Its period is at least double that of the other bubbles. Very similar effects are seen when the number of bubbles is increased. Figure 9 shows a 21-bubble configuration, where again growth occurs without too much interference between the bubbles. However, collapse proceeds from the outer bubble shells towards the inside, indicating a cloud period of oscillation much larger than that of individual bubbles [7].

Bubble Dynamics on the Axis of a Vortex

Consider now the case of a bubble on the axis of a vortex line. At $t = 0$ there is an excess internal pressure and the bubble starts to grow. During the growth phase the bubble elongates along the vortex axis, then starts its collapse from a signif-

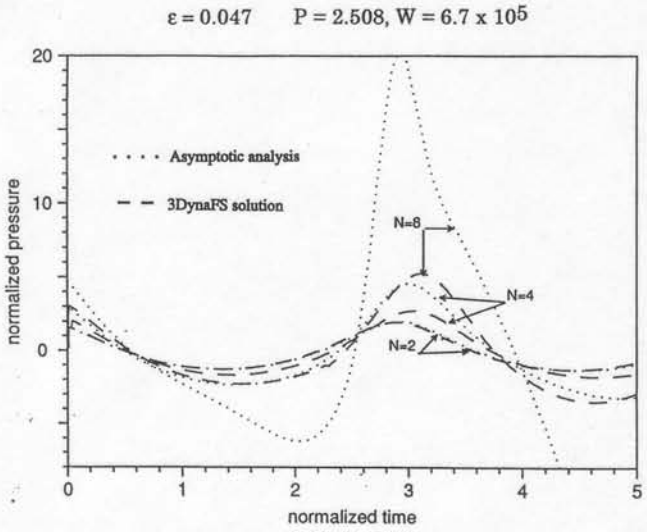

Figure 7: Comparison of the pressures at the cloud center predicted by 3DYNAFS and the asymptotic analysis code. $\epsilon = R_{max}/l_0 = 0.047$. Pressures are normalized by maximum value for isolated bubble [9].

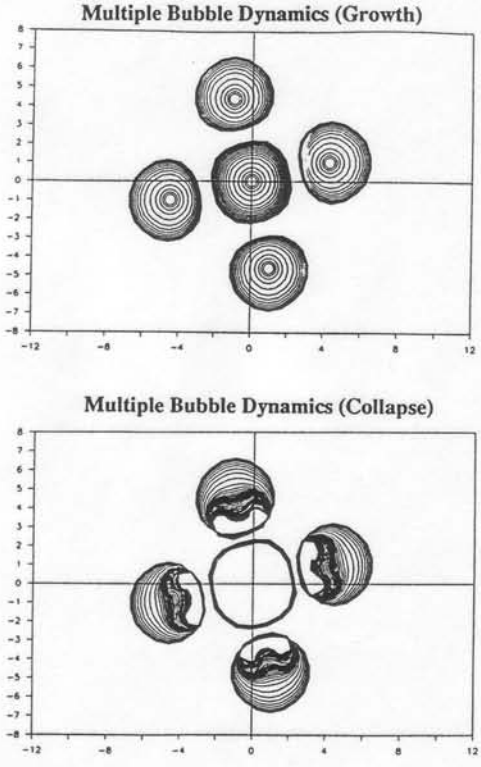

Figure 8: Growth and collapse of 5 bubbles having the same initial size and internal pressure. Influence of the initial bubble geometry distribution on dynamics. $\epsilon = 0.474$, $P_{go}/P_{amb} = 283$ [9].

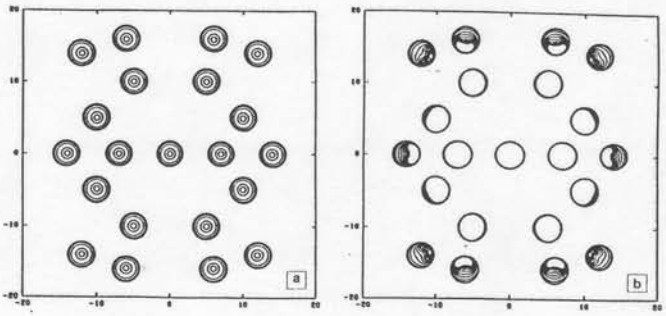

Figure 9: Simulation of the dynamical interactions between a cloud of 21 bubbles using **3DynaFS** on a Cray. Two planes of symmetry are used. Each bubble has 102 nodes and 200 panels. a) Growth. b) Collapse [9].

icantly elongated shape [10]. As shown in Figure 10*a*, this elongation is not the key parameter to the subsequent bubble behavior. If the rotation velocity is neglected, the collapse would proceed as for elongated bubbles with two opposing jets formed at the bubble points along the axis (Fig. 10*a*, top). However, the opposite effect with a radial jet forming is obtained when the rotation in the vortex flow is included. The bottom of Figure 10*a* illustrates this for particular values of the vortex circulation, Γ, and the normalized viscous core radius, $\overline{R_c} = R_c/R_{max}$.

In Figure 10*b*, the initial pressures inside the bubbles are taken to be larger than the pressure on the vortex axis, and the bubbles are left free to adapt to this pressure difference. For a given value of Γ, the bubble behavior strongly depends on $\overline{R_c}$. In all cases where $\overline{R_c} < 1$ it appears that the bubble tends to adapt to the vortex tube size. This could lead to various bubble shapes as shown in Figures 10*b* ending up with a very elongated bubble with a wavy surface for small values of $\overline{R_c}$. The figure shows bubble contours at various times during growth and collapse for various values of R_c, and initial bubble pressures. Also shown are selected 3D shapes of the bubbles at various times. It is apparent from these figures that during the initial phase of the bubble growth, radial velocities are large enough to overcome centrifugal forces and the bubble first grows almost spherically. Later on, the bubble shape starts to depart from the spherical and adapts to the pressure field. The bubble then elongates along the axis of rotation. Once the bubble has exceeded its equilibrium volume, bubble surface portions away from the axis – high pressure areas – start to collapse, or to return

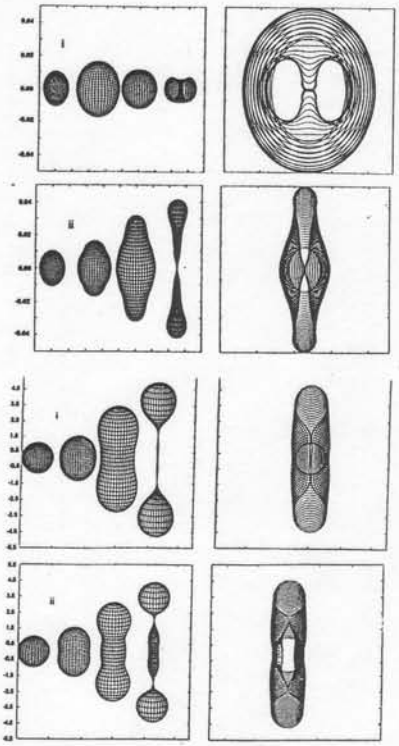

Figure 10: Bubble dynamics on the axis of a vortex line. Left side shows 3D shapes at selected times. Right side shows bubble contours at increasing times. a) Initial elongation ratio of 3, $p_i/p_\infty = 3.27$. i) No swirl, ii) $\Omega = 0.56$, $R_c/R_{max} = 3$. b) $\Gamma = 0.005m^2/s$, $R_o = 100\mu m$. i)$p_i/p_\infty = 2$, $R_c/R_o = 1$, ii) $p_i/p_\infty = 1$, $R_c/R_o = 1$ [10].

rapidly towards the vortex axis. To the contrary, points near the vortex axis do not experience rising pressures during their motion, and are not forced back towards their initial position, thus continuing to elongate along the axis. As a result, a constriction appears in the mid-section of the bubble. The bubble can then separate into two or more tear-shaped bubbles. This splitting of the bubbles is the main contributor to cavitation inception noise which is used as a means of detecting cavitation.

Cavitation Dynamics on Propeller Blades

The precise condition under which a cavity forms on a solid boundary is not yet well understood. Recently in a careful experiment Morch & Song [17] have shown that a perfect contact between a solid boundary and the liquid cannot exist and that nanoscopic air cavities remain all along any wetted solid surface, thus forming potential cavitation areas. This justifies the use of a cavity model that postulates development and growth of a cavity when the pressure at the solid surface drops below some critical pressure, p_c. Using the same BEM method described above the foil or propeller blade is discretized into nodes and panels on which the condition of no cross-flow is satisfied. The problem is then solved for a given imposed incidence and velocity of the liquid "at infinity" far from the blade. Then, if the pressure at any panel of the solid surface is found to be below the critical pressure p_c, that panel is made a free surface that can move away from the solid surface. This newly created cavity panel is an interface on which we satisfy dynamic pressure conditions such as described above. The space volume between the initial body surface and the freely moving free surface forms the cavity of volume $\mathcal{V}$ that grows and collapses on the body. The cavity surface also moves with the local fluid $\mathbf{u}$ subject to the condition that no cavity point can penetrate the physical solid surface of the body. During local cavity collapse a free surface point that touches the solid surface underneath is made a solid node again. Some example results are shown in Figures 11.a . The simulations were performed using 3DYNAFS and are compared to experiments of development of sheet cavitation on an elliptical planform hydrofoil of NACA 0012 cross-section [18] in Figure 11.b.

CONCLUSIONS

In this contribution we have reviewed various aspects of cavitation inception and bubble dynamics. A few models for bubble growth and collapse were then presented, including non spherical bubble dynamics. The influence of relative liquid bubble flow, multibubble interactions and the presence of non uniform flow fields were also briefly considered. Finally, the extension of the model to large scale cavity inception and dynamics was presented. The comparison of the results with available experimental observations shows that the Boundary Element Method is a promising method for cavitation dynamics simulation.

ACKNOWLEDGMENTS

I am indebted to the Lebanese National Council of Scientific Research for its support when I was a PhD student on the subject of cavitation 23 years ago, support without which I would not have been able to pursue a research career. Several parts of the work described in this paper were conducted under support form the United States Office of Naval Research. My thanks also go to many colleagues at DYNAFLOW who have made significant contributions to this work.

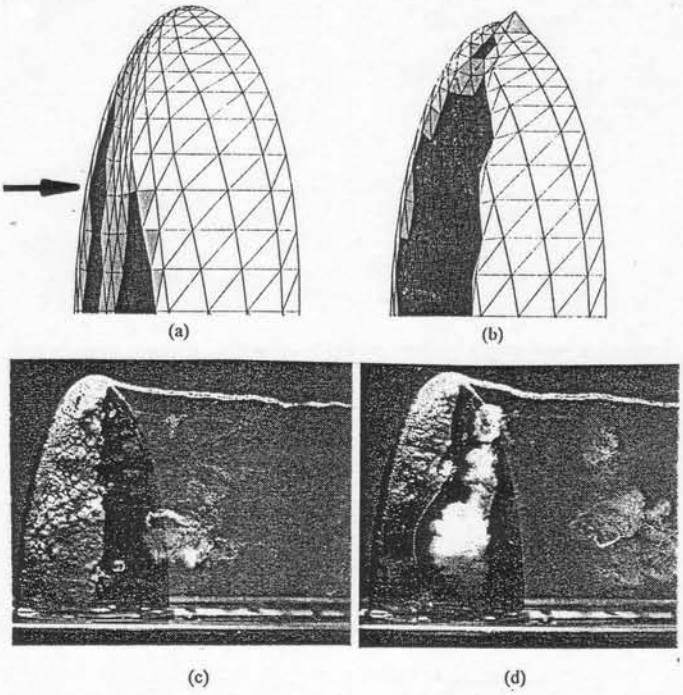

Figure 11: Cavitation on NACA012 hydrofoil. Simulation using 3DYNAFS with dark panels indicating a cavity, a) $\alpha = 8^o$, $V = 10m/s$, $\sigma = 0.5$. b) $\alpha = 12^o$, $V = 10m/s$, $\sigma = 1.3$, c) d) Experimental observation from [18] $\alpha = 10^o$, $V = 10m/s$, $\sigma = 1.5$ at two instants.

.

References

1. BESANT, W. H., "Hydrostatics and Hydrodynamics," Art. 158, Cambridge Univ. Press, London, 1859.

2. RAYLEIGH, LORD, "On the Pressure Developed in a Liquid During Collapse of a Spherical Cavity," Phil. Mag., 1917;34:94-98.

3. BROWN, B. AND GOODMAN, J.E., "High Intensity ultrasonics - Industrial Applications," Life Books ltd., London, 1965.

4. CHAHINE, G.L., AND JOHNSON, JR., V.E.,"Mechanics and Applications of Self-Resonating Cavitating Jets," ASME International Symposium on Jets and Cavities, WAM, Miami, Florida, 1985;FED-Vol.31:21-35.

5. CHAHINE, G.L., JOHNSON, JR., V.E., LINDENMUTH, W.T., AND FREDERICK, G.S. "The use of Self-Resonating Cavitating Water Jets for Underwater Sound Generation", Journal of the Acoustical Society of America, 1985; 77-1:113-126.

6. HAMMITT, F. G., "Cavitation and Multiphase Flow Phenomena," McGraw-Hill International Book Company, N.Y., 1980.

7. YOUNG, F. R."Cavitation," McGraw Hill Book Company, N.Y., 1989.

8. CHAHINE, G.L,"Dynamics of the interaction of non-spherical cavities," in "Mathematical approaches in hydrodynamics," ed. T. MILOH, *SIAM, Philadelphia*, 1991;51-68

9. CHAHINE, G.L. AND DURAISWAMI, R. "Dynamical Interactions in a Multi-Bubble Cloud." ASME, Journal of Fluids Engineering, 1992;Vol. 114: 680–687,

10. CHAHINE , G. L., "Bubble Interaction with Vortices," Chap. 18 in "Fluid Vortices," ed. Sheldon Green, Kluwer Academic Publishers, 1995 .

11. CHAHINE, G.L., KALUMUCK, K. M., AND DURAISWAMI, R., "Coupling of a Fluids BEM Code with a Structural FEM Code for Fluid-Structure Interaction Simulation," BE XV, Vol.1: Stress Analysis, Ed. C.A. Brebbia and J.J. Rencis, CMP, Elsevier, 1993; 581-597.

12. LAUTERBORN, W., "Cavitation and Coherent Optics," in Cavitation and Inhomogeneities in Underwater Acoustics, ed. W. Lauterborn, Springer Verlag, 1980;3-13.

13. CHAHINE, G.L., "Etude Locale du Phénomène de Cavitation. Analyse des Facteurs Régissant la Dynamique des Interfaces," Docteur d'Etat és-Sciences Thesis, Université Pierre et Marie Curie, April, 1979.

14. SARKAR, K., CHAHINE, G.L., AND DURAISWAMI, R. "Three-Dimensional Bubble-Vortical Flow Interaction — A Numerical Study," submitted J. Fluid Mech., 1996.

15. CHAHINE, G. L., "Experimental and Asymptotic Study of Non-spherical Bubble Collapse," Applied Scientific Research, 1982;38:187-197.

16. CHAHINE, G.L., "Cloud Cavitation: Theory," 14th Symposium on Naval Hydrodynamics, Ann Arbor, Michigan, National Academy Press, Washington, D.C., 1983:165-195.

17. MORCH, K. A., AND SONG, J. P."Cavitation Nuclei at Solid-Liquid Interfaces," Cavitation: Proceedings of the Institution of Mechanical Engineers, 1-7, 1992.

18. BOULON, O., "Etude Expérimentale de la Cavitation de Tourbillon Marginal. Effets Instatinnaires, de germes et de Confinement, Thesis, Institut National Polytechnique de Grenoble, April 1996.